ELSEVIER

Earth and Planetary Science Letters 186 (2001) 125–141

EPSL

www.elsevier.com/locate/epsl

The 10Å phase: a high-pressure expandable sheet silicate stable during subduction of hydrated lithosphere

Patrizia Fumagalli [a,*], Lars Stixrude [b], Stefano Poli [a], Don Snyder [b]

[a] *Dipartimento di Scienze della Terra, Università degli Studi di Milano, Via Botticelli 23, 20133 Milan, Italy*
[b] *Department of Geological Sciences, University of Michigan, 425 E. University Ave., Ann Arbor, MI 48109, USA*

Received 29 September 2000; received in revised form 8 January 2001; accepted 14 January 2001

Abstract

H_2O storage and release in deep subducting lithosphere is controlled by complex reaction suites involving a variety of hydrous phases. As a result of its relatively large thermal stability and intermediate composition, the 10Å phase ($Mg_3Si_4O_{10}(OH)_2{\cdot}nH_2O$) has been regarded as a relevant H_2O reservoir in a wide range of rock compositions and mineral assemblages. High-pressure syntheses of the 10Å phase were carried out at 6.7 GPa and 650°C under fluid-saturated conditions in a Walker-type multi-anvil apparatus, from 5 min to 430 h. X-ray powder diffraction of large platy hexagonal crystals of the 10Å phase (up to 100 μm) were indexed on the basis of a trioctahedral-type structure. Long-term run products (>110 h) reveal sensitivity of the 10Å phase to treatment with acetone leading to the appearance of diffractions at greater *d*-spacings (10.2–11.6 Å) with respect to the basal peak of the 10Å phase (9.64–10.07 Å). This swelling behavior is strongly related to synthesis run duration. The Raman spectrum of the 10Å phase at frequencies less than 800 cm^{-1} shows a strong similarity to talc. In the Si–O stretching region (800–1100 cm^{-1}), the 10Å phase exhibits three modes (909, 992 and 1058 cm^{-1}), as compared to two in talc. The bending mode of water (v_2) is found at 1593 cm^{-1}. In the OH stretching region, peaks at 3593, 3622 and 3668 cm^{-1} were observed. The acetone treated sample shows a C–H stretching mode at 2923 cm^{-1} while the double bond C=O signal is absent. The swelling behavior of the 10Å phase is interpreted as due to intercalation of acetone with pre-existing interlayer water. The efficiency of this process is dependent on the amount of the interlayer water which in turn depends on run duration. The relation between the response to acetone treatment and run duration is therefore interpreted as a time-dependent hydration of the 10Å phase. The fractions transformed from non-expandable to expandable fractions was fitted to the Avrami empirical law which suggests that kinetics are mainly controlled by diffusion rather than phase boundary reactions. The ability to accommodate variable amounts of H_2O makes the 10Å phase a major H_2O sink whenever a hydrous phase such as chlorite and serpentine breaks down during prograde transformations in the subducted lithosphere. Under H_2O-saturated conditions, a fully hydrated 10Å phase occurs; when H_2O-undersaturated conditions prevail, a H_2O-deficient 10Å phase incorporates the volatile component available. The exchange capacity of interlayer molecules in the 10Å phase structure opens new scenarios on the control of fluid compositions escaping from subducted slabs.

Keywords: subduction; 10Å phase; hydrous phase; experimental studies; high pressure

* Corresponding author. Present address: Department of Geological Sciences, University of Michigan, 425 E. University Ave., Ann Arbor, MI 48109, USA. Tel.: +1-734-647-9391; Fax: +1-734-763-4690; E-mail: patrizia.fumagalli@umich.edu

0012-821X/01/$ – see front matter
PII: S0012-821X(01)00238-2

1. Introduction

Subducting slabs undergo dehydration that triggers most of the petrological processes occurring at convergent margins. Several hydrous phases have been regarded as possible candidates for carrying water deep into the Earth's mantle. Talc is expected to occur in a large range of mineral assemblages in rock compositions ranging from altered peridotites [1] to Mg-gabbros [2], to pelitic blueschists [3]. Talc transforms to the hydrous 10Å phase at pressures between 3 and 5 GPa through the reactions talc+H_2O = 10Å phase and, at higher pressures, through the fluid-absent reaction talc = 10Å phase+enstatite+coesite [4–6]. The fluid-absent formation of talc is significant because it means that the 10Å phase is a candidate for transport, storage and release of water in subduction zones to depths exceeding the stability field of talc. Moreover, the occurrence of the 10Å phase is not restricted to the ternary MgO–SiO_2–H_2O system: we recently showed [7,8] the occurrence of an aluminous 10Å phase in synthetic peridotites at 5.2 GPa, 680°C, beyond the stability field of chlorite and/or talc and/or antigorite.

Despite the potential significance of the 10Å phase, uncertainty remains regarding its structure and composition. The 10Å phase, first synthesized by Sclar et al. [9], is a phyllosilicate chemically analogous to talc but with excess water: the chemical formula may be represented as $Mg_3Si_4O_{10}(OH)_2{\cdot}nH_2O$. The amount of water is uncertain, previous results indicate $n=2$ [4], $n=1$ [10] and $n=0.65$ [11]. Apart from the study of Yamamoto and Akimoto [4] these values were obtained by weight-loss experiments.

The stability of the 10Å phase has been questioned by Wunder and Schreyer [11]. They constrained the occurrence of the 10Å phase to high water content (>30 wt%) and short time runs (<4 h). More recently the same authors constrained the stability field of the 10Å phase to a temperature less than 580°C at 7 GPa [12]. However, recent in situ observations of the formation of the 10Å phase through both water present and water-absent reactions at mantle pressures and temperatures [6] support the occurrence of the 10Å phase in equilibrium.

The 10Å phase is identified from the X-ray powder diffraction pattern by the basal plane spacing which may range from 9.81 to 10.6 Å [4,9,10,13]. The value of the basal *d*-spacing is substantially larger than that of talc (9.34 Å), but similar to that of 2:1 trioctahedral micas such as phlogopite [10]. However, the source of the net charge required for a mica-type structure and the nature of interlayer cations in the 10Å phase are still under debate. On the basis of infrared (IR) spectroscopy and thermal analysis, Bauer and Sclar [10] proposed that water molecules occupy the interlayer 12-coordinated site of a mica-like structure and interact with hydroxyl groups of the octahedral layers. This interaction leads to the formation of hydronium (H_3O^+) according to the relation $H_2O+OH^- \rightarrow H_3O^+ + O^{2-}$ and to the new structural–chemical formula $H_3O^+Mg_3Si_4O_{10}(OH)$. The presence of hydronium was inferred on the basis of a peak in IR absorption at 1700–1720 cm^{-1}. High-pressure differential thermal analysis carried out by Miller et al. [14] provided evidence for a resonating proton model of water storage: oxygen ions are incorporated in the 12-coordinated site and balanced by two resonating protons. This mechanism leads to the momentary formation of OH, H_2O and H_3O^+.

Here we report the results of new X-ray diffraction experiments on the 10Å phase samples, both treated with organic liquids and untreated. We also report the first Raman spectroscopic investigation of this phase. On the basis of these results, we propose a new model of the structure of the 10Å phase and we discuss the role of this unusual expandable high-pressure phase in controlling H_2O recycling in subduction zone environments.

2. Materials and methods

Stoichiometric gels ($MgO:SiO_2 = 3:4$) were used as starting materials in order to synthesize the 10Å phase. Gels were prepared following the method of Hamilton and Henderson [15] using tetraethylorthosilicate as the silica source, pure Mg, nitric acid and ammonium hydroxide. High-pressure syntheses of the 10Å phase were carried out at 6.7 GPa and 650°C in a Walker-

type multi-anvil apparatus at the Dipartimento di Scienze della Terra, Milan. All experiments were performed under fluid-saturated conditions. Since the stability of the 10Å phase has been questioned [11] we performed experiments with different durations, from 5 min to 430 h. Experimental conditions are summarized in Table 1. Gold and platinum capsules (up to 4.6 mm outer diameter and length from 3.5 to 4.5 mm) were welded after being loaded with 10–25 mg gel and 15 wt% distilled water. Tungsten carbide cubes of 32 mm edge length and 17 mm truncation edge length were used. Pressure cells were made of prefabricated MgO octahedra (containing 5 wt% of Cr_2O_3) with a 25 mm edge length. Assemblies were composed of a stepped graphite heater, MgO spacers and an axial thermocouple (Pt–$Pt_{90}Rh_{10}$, S-type) insulated by a mullite ceramic and placed in direct contact with the capsule. Graphite discs on both ends of the assembly provided electrical contact with the WC cubes. Pressure calibration was performed both at room temperature, using the phase transitions Bi I–II, Bi III–V (respectively at 2.55 and 7.7 GPa), and at 1000°C, the coesite–stishovite, and $CaGeO_3$ garnet–perovskite transitions occurring, respectively, at 8.7 GPa [16] and 6.1 GPa [17]. Pressure uncertainties, which largely depend on the accuracy of the calibrant reaction, were assumed to be ±4% [7]. Temperature was considered accurate to ±20°C without taking into account any effect of pressure on the emf of the thermocouple.

Run products were first characterized by X-ray powder diffraction on a Philips APD 1000 diffractometer and inspected on backscattered and secondary electron images. An ARLK microprobe with six spectrometers was used for microanalysis. Beam conditions were set to 15 kV and 20 nA. Silicates were used as standards and data processed with a ZAF correction procedure. Run products were treated with acetone at room conditions and differences in the XRD pattern before and after the treatment were observed.

Raman spectra were collected at the micro-Raman laboratory of the University of Michigan. The excitation source is provided by a 6 W Ar-ion continuous-wave laser from which the 514.5 nm line is used. An Olympus BH-2 microscope equipped with a Mitatoyo 50× objective is used to focus the laser to a spot of 2 μm on the single crystal. The scattered radiation is analyzed with a Spex 1250 spectrometer equipped with a 600 g/mm holographic grating and collected by a cooled CCD detector. Raman shifts ranging from 50 to 4000 cm^{-1} were measured with laser power ranging from 0.3 to 1 W. Up to 11 accumulations of 180 to 650 s typical duration were integrated.

Table 1
Pressure, temperature and run time for high-pressure synthesis experiments on the 10Å phase

Run	P_{oil} (bar)	P (GPa)	T (°C)	Time
Ta9	350	6.7	650	5 min
Ta8	350	6.7	650	1 h
Ta11	350	6.7	650	28 h
Ta1	270	5.2	680	115 h
Ta3	350	6.7	650	311 h
Ta7	350	6.7	650	361 h
Ta14	350	6.7	650	430 h

3. The structure of the 10Å phase: X-ray data

The 10Å phase was recognized by X-ray powder diffractometry mainly on the basis of the quite sharp basal peak at $d = 9.93$–10.07 Å. Short runs (< 110 h) lead to the formation of tiny aggregates of microcrystalline powder (> 1 μm). Increasing run durations produce a well-crystallized 10Å phase up to 100 μm in size and of platy hexagonal habit (Fig. 1). The well-crystallized nature of the 10Å phase in our long-term runs is also supported by preliminary transmission electron microscopy investigations not included here but in progress (R. Wirth, personal communication). However, attempts to collect single crystal precession data revealed diffraction stricks along the reciprocal direction c^*, suggesting the occurrence of stacking faults. The collection of single crystal data is further complicated by the sensitivity of the 10Å phase to most organic liquids (e.g. glues). Further syntheses of single crystals suitable for structural analyses are in progress. Microanalysis carried out both on short and long run products reveal

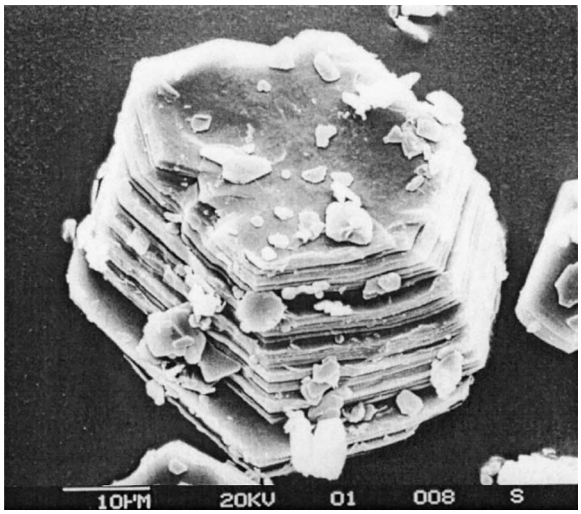

Fig. 1. SEM image of platy hexagonal 10Å phase synthesized at 6.7 GPa, 650°C for 430 h.

a ratio $MgO:SiO_2$ of 3:4, this corresponds to the stoichiometry of talc in which the 2:1 layers do not carry any net charge. However X-ray powder diffraction patterns suggest that the 10Å phase is better indexed on the basis of a phlogopite instead of a talc structure. In Fig. 2 the diffraction pattern of the 10Å phase synthesized at 6.7 GPa and 650°C for 430 h is compared with the diffraction patterns calculated for 2:1 trioctahedral phyllosilicate structures: a talc-like and a mica-like model structure with two water molecules pfu in the interlayer. The two structures differ primarily in the type of stacking: alignment of tetrahedral sheets across the interlayer in micas creates a 12-coordinated site that is absent in the talc. It should be noted that the X-ray diffraction pattern is insensitive to either the number or detailed positions of hydrogens. Therefore the details of the hydrous portion of the model structure relies primarily on other types of data. Details on the occurrence of water molecules in the interlayer are further justified in subsequent discussions.

X-ray powder diffraction data are shown in Table 2. Reflections are indexed on the basis of the

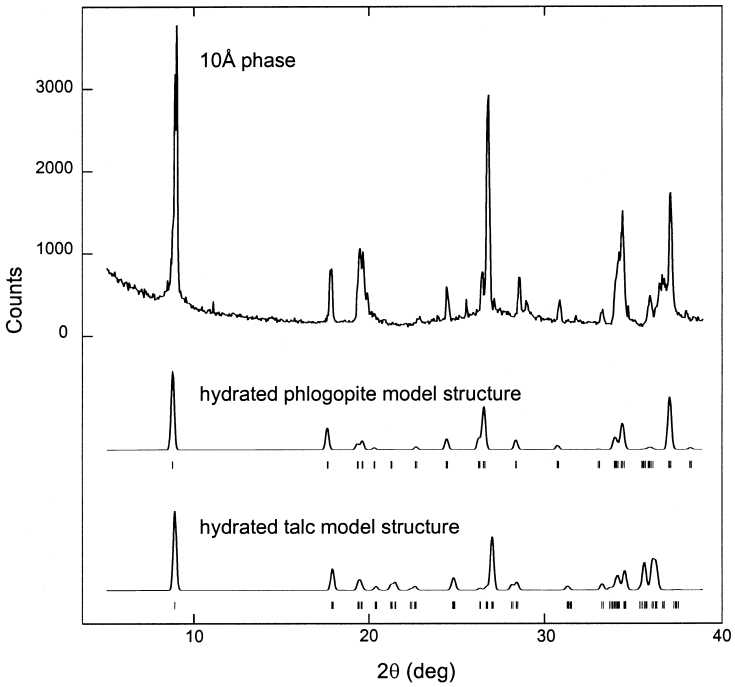

Fig. 2. X-ray diffraction pattern of 10Å phase. The two diffraction patterns at the bottom calculated for hydrated phlogopite and hydrated talc model structures are discussed in the text.

model phlogopite-type stacking discussed above. Preliminary Rietveld refinement results in the following lattice parameters: $a = 5.316(2)$ Å, $b = 9.200(3)$ Å, $c = 10.196(3)$ Å and $\beta = 99.99(3)°$. Our diffraction data are generally in good agreement with peak locations and relative intensities as reported by Bauer and Sclar [10]. The one exception is the relative intensity of the 020 diffraction at 4.56 Å which is lower in this study compared with that of Bauer and Sclar [10]. The relative intensities reported by Yamamoto and Akimoto [4] are discrepant with the present results and those of Bauer and Sclar [10]. The data of Yamamoto and Akimoto [4] may be affected by a strong preferred orientation as indicated by the high intensity of 001 diffractions and the extremely low intensities ($< 10\%$) of the remaining peaks.

We found that treatment of the sample with organic liquids had a substantial effect on the X-ray diffraction pattern, especially for large *d*-spacings. The effect of treatment was not the same for all samples, but depended on the length of the synthesis run. In Fig. 3 the low-angle portion of diffraction patterns of the 10Å phase synthesized at 6.7 GPa and 650°C for 430 h before and after acetone treatment are shown. The treated sample shows a broad feature, not present in the untreated sample, at large *d*-spacings (11.60–11.10Å). This apparent swelling behavior is strongly related to synthesis run duration. Three samples obtained with the same composition, and the same pressure and temperature conditions (6.7 GPa and 650°C) but quenched at different times (1, 111 and 311 h) and then treated at room conditions with acetone are compared in Fig. 4. The basal peak of talc, indicated with the dashed line, was not observed in any experiment. While long-term run products show a strong evidence of interaction of the 10Å phase with acetone, short-term run products are less affected by the solvent. Both broad and sharp peaks

Table 2
X-ray powder diffraction data for the 10Å phase. d_{calc} by Rietveld refinement on the basis of a trioctahedral mica model structure

d_{obs} (Å)	I/I_0	*hkl*	d_{calc} (Å)	d_{obs} (Å)	I/I_0	*hkl*	d_{calc} (Å)
9.93	100	001	9.89	2.002	21	−223	2.025
4.98	22	002	4.985			005	2.004
4.564	28	020	4.571	1.986	8	133	1.988
4.511	27	110	4.522	1.902	6	203	1.904
3.641	16	−112	3.639			−134	1.903
3.373	20	022	3.377			043	1.892
3.329	78	003	3.332	1.732	9	150	1.733
3.126	19	112	3.131			−241	1.733
2.899	11	−113	2.903	1.694	9	044	1.693
2.695	9	023	2.697	1.668	20	204	1.670
2.629	30	−201	2.639			−135	1.669
		130	2.638			−152	1.668
2.608	40	−131	2.608	1.643	17	311	1.642
		200	2.610			−313	1.641
2.497	13	131	2.498	1.609	6	152	1.610
		113	2.513	1.596	6	−243	1.610
		004	2.503	1.565	6	026	1.570
2.462	17	−202	2.499			242	1.577
2.422	46	−132	2.423			−153	1.576
2.375	8	−114	2.347	1.531	57	060	1.531
2.289	10	040	2.294			−331	1.532
		−221	2.289	1.514	23	061	1.514
2.256	10	220	2.269			−332	1.515
2.162	18	202	2.166				
		−133	2.165				

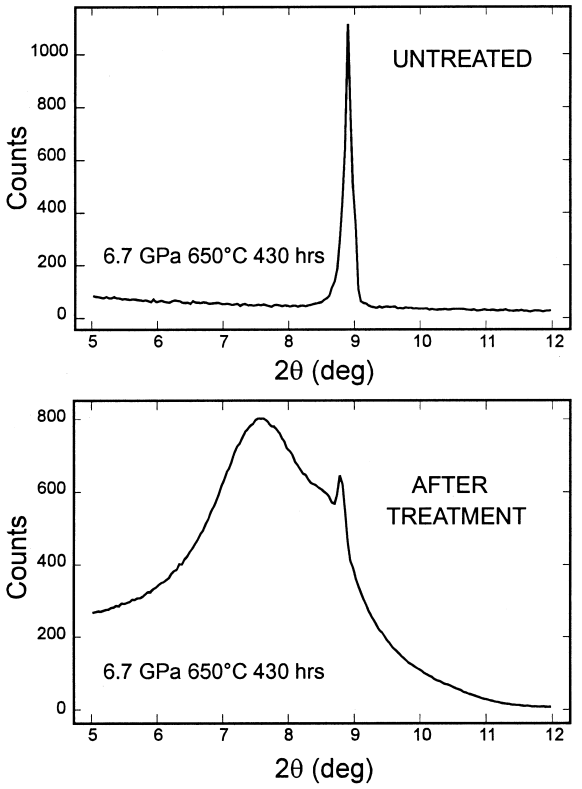

Fig. 3. Expansion after acetone treatment of the basal *d*-spacing of the 10Å phase observed in X-ray diffraction patterns. The figure refers to the 10Å phase synthesized at 6.7 GPa, 650°C and for 361 h.

show a shift of the *d* value with time: the broad peak ranging from 10.2 to 11.6 Å and the sharp peak varying from 9.64 to 10.07 Å.

4. The structure of the 10Å phase: micro-Raman spectroscopy data

Raman spectra of an untreated 10Å phase were collected on crystals (up to 100 μm) synthesized at 6.7 GPa and 650°C for 430 h. Samples from long-term syntheses (Ta14: 430 h) were preferred because short duration runs lead to aggregates of a poorly crystallized 10Å phase (<1 μm). Crystals were placed on a thin glass slide; the incident laser was perpendicular to the (001) plane. The Raman spectrum of the 10Å phase shows a strong similarity to talc and is less comparable with phlogopite [18]. In order to aid in peak assignments, we compare our Raman spectra to that of talc in detail. To this end, we synthesized a specimen of talc in the system $MgO–SiO_2–H_2O$ at 2.2 GPa and 700°C in a single stage piston cylinder at the Dipartimento di Scienze della Terra of Milan. In Table 3 the frequencies and assignments of Raman bands observed in talc and the 10Å phase are shown and compared to phlogopite.

The low- and medium-frequency region of the 10Å phase is shown and compared to that of talc

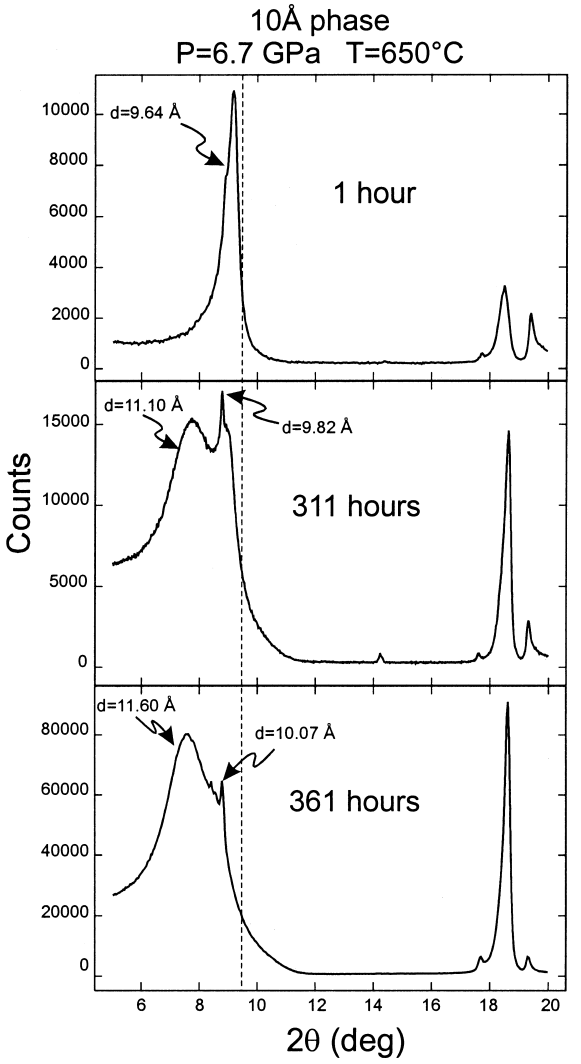

Fig. 4. The swelling behavior of the 10Å phase is time-dependent. The dashed line indicates the position of the talc basal diffraction. See text for further comments.

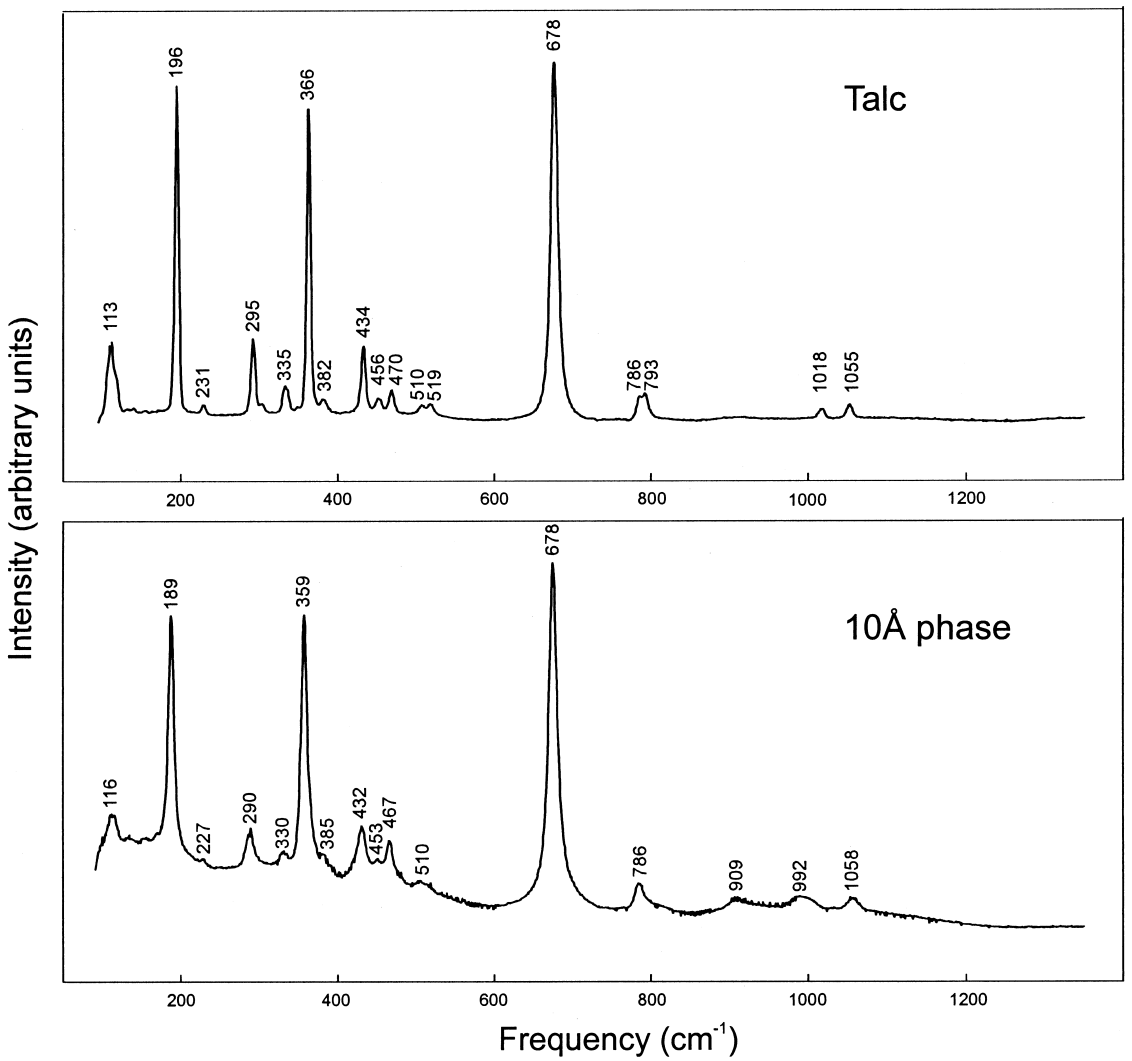

Fig. 5. Raman spectra up to 1300 cm^{-1} of the 10Å phase compared to that of talc. Note the intensity of peaks around 1000 cm^{-1}. The spectrum of the 10Å phase refers to the run product obtained at 6.7 GPa, 650°C and for 430 h (Ta14). See text for details.

in Fig. 5. The spectra in this frequency range (<800 cm^{-1}) are very similar. Mg–OH^- vibrations in talc have been assigned to the frequencies at 113, 197 and 471 cm^{-1} ([19] and references therein). In the spectrum of the 10Å phase the frequencies of Mg–OH^- vibrations are slightly shifted with respect to those in talc and occur at 116, 189 and 467 cm^{-1}. Talc and the 10Å phase show Si–O–Si bending vibrations at the same frequencies: 432 and 678 cm^{-1}. Modes observed in the 10Å phase at 510 and 453 cm^{-1} are assigned to OH vibrations, in accordance with the appearance of these modes in talc at 511 and 456 cm^{-1}. In the region between 800 and 1100 cm^{-1} the Raman spectrum of the 10Å phase differs from that of talc. In talc the 1018 and 1055 cm^{-1} modes are assigned to Si–O stretching within the layer (Si–O–Si) and to stretching of the non-bridging Si–O bond, respectively [19]. In the spectrum of the 10Å phase both modes are present,

but are shifted in frequency (996 and 1058 cm^{-1}) and an additional peak appears at a lower frequency (909 cm^{-1}).

The high-frequency portion of the Raman spectrum allows us to explore hydrogen bonding and speciation in the 10Å phase. In the 10Å phase a peak is observed at 1593 cm^{-1} that is absent in talc (Fig. 6). In the OH stretching region, four peaks are observed in the 10Å phase; two sharp peaks at 3593 and 3622 cm^{-1}, and two broad peaks at 3267 and 3668 cm^{-1} (Fig. 7). In contrast, for talc, we observe only one mode in this region at 3677 cm^{-1}, in agreement with previous work. This mode is assigned to stretching of the OH of the octahedral layer.

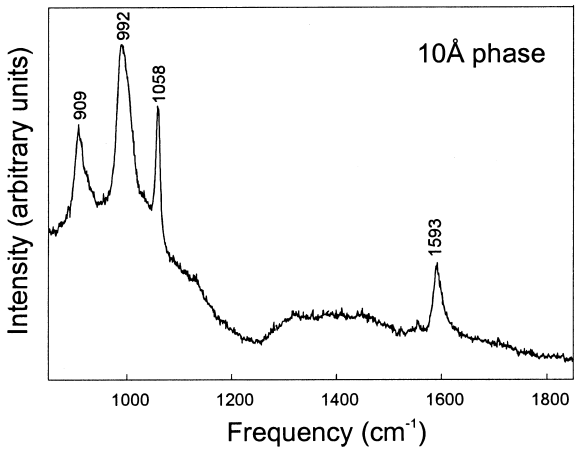

Fig. 6. Raman spectrum of the 10Å phase (Ta14) in the region 800–1900 cm^{-1}. The intensity of the peak at 1593 cm^{-1}, assigned to the water bending mode (see text), is compared to peaks around 1000 cm^{-1} (see also Fig. 5).

5. Raman spectra on treated 10Å phase: interaction with acetone

The 10Å phase synthesized at 6.7 GPa, 650°C for 430 h was treated with acetone and Raman

Table 3
Raman frequencies for the 10Å phase and talc and relative assignments. Observed data are compared to phlogopite [18]

Phlogopite	Talc	10Å phase	Assignments
	113	116	MgOH
199	196	189	MgOH
234	231	227	
282	295	290	
326	335	330	
373	366	359	
	382	385	
	434	432	Si–O–Si bending
	456	453	OH transition
	470	467	MgOH
513	510	510	OH liberation
641	519		
684	678	678	Si–O–Si bending
712	786	786	
801	793		
		909	Si–O–Si symmetric stretching
1034	1018	992	Si–O–Si symmetric stretching
1094	1055	1058	Si–O stretch
		1593	water bending mode (ν_2)
		3267	first overtone ($2\nu_2$) of the fundamental water bending vibration
		3593	OH of interlayer water
		3622	OH stretching of structural hydroxyls
3724	3677	3668	OH of interlayer water

spectra were collected on the treated samples. Since the treated 10Å phase was comparatively unstable under the laser we collected the spectra at lower power (<0.5 W) and with smaller accumulation and integration times. As a result, the signal to noise ratio of the Raman spectra of the treated samples is inferior to that of the untreated samples. Nevertheless, the Raman spectrum in the region from 100 to 800 cm^{-1} presents the same major features as observed in the untreated sample (Fig. 8a). Between 900 and 1250 cm^{-1} a broad low-intensity band may obscure the presence of peaks related to Si–O–Si and SiO^{-} stretching (not shown). A mode is observed at 1593 cm^{-1} at the same frequency as in the untreated sample (Fig. 8b). The high-frequency region (Fig. 8c) shows a new peak at 2923 cm^{-1}. The OH stretching region of the treated samples is very similar to that of the untreated one, showing three peaks at 3593, 3622 and 3677 cm^{-1}. While the first two are at the same frequencies, the last one is shifted to slightly higher frequencies. Furthermore the relative intensities of the three peaks are different: the highest frequency peak is the most intense, and the shoulder on the high-frequency side is no longer present. A band at lower frequency is still present, although it is much broader, ranging from 3000 to 3600 cm^{-1}.

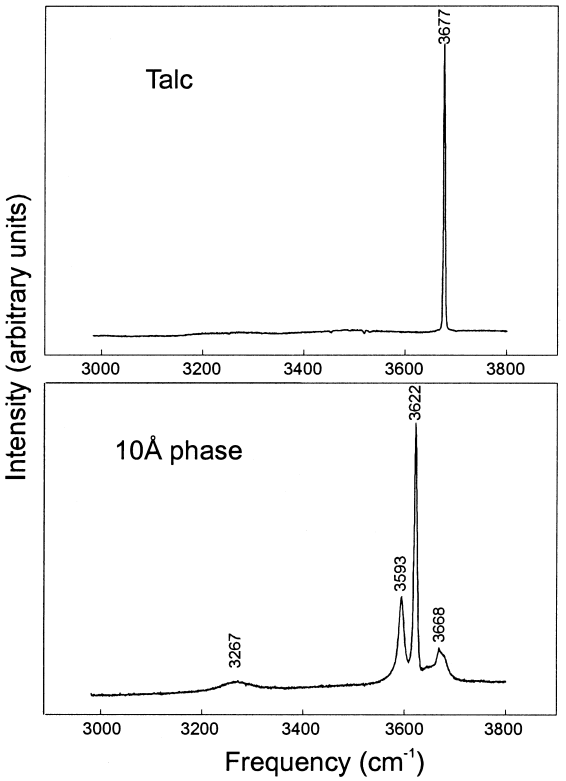

Fig. 7. Raman spectra of the OH stretching region of the 10Å phase (Ta14) compared to that of talc. While talc presents only a sharp peak at 3677 cm^{-1} (hydroxyls coordinated by magnesium), the 10Å phase shows a more complex hydrogen configuration.

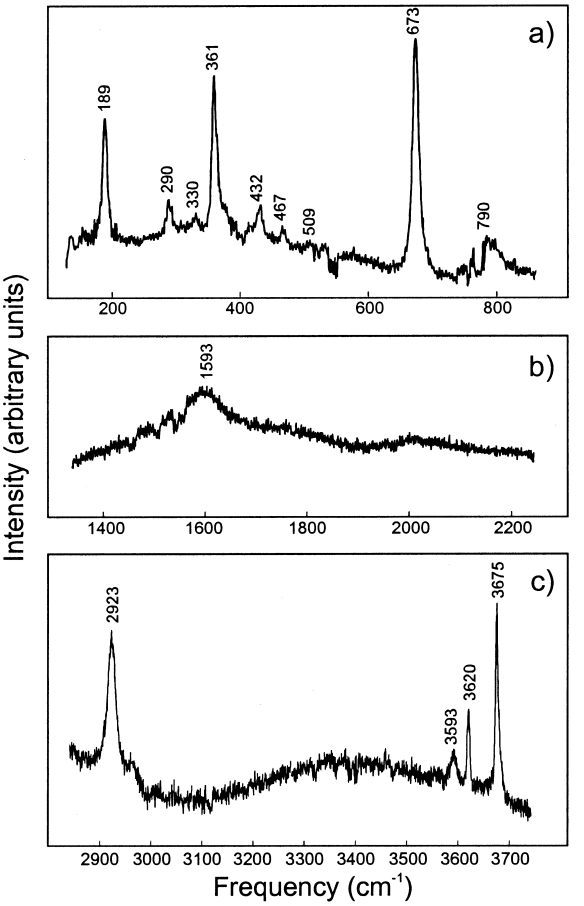

Fig. 8. Raman spectra of acetone treated 10Å phase (Ta14). (a) Region from 100 to 900 cm^{-1}; (b) region from 1300 to 2300 cm^{-1}. The bending mode of molecular water appears at 1593 cm^{-1}. No signal for the C=O vibration has been observed at 1708 cm^{-1}. (c) OH stretching region. The peak at 2923 cm^{-1} is associated to CH_3 vibrations due to acetone entering the structure.

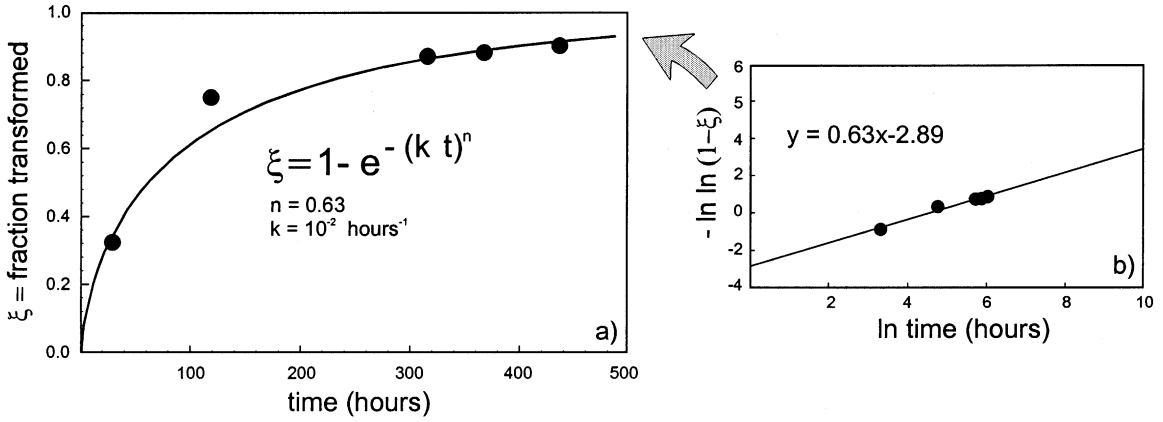

Fig. 9. (a) Fraction transformed (ξ) versus time. The fraction transformed ($\xi = I_b/(I_b+I_s)$) is evaluated by fitting the integral areas of broad and sharp basal peaks (I_b and I_s, respectively) of each different run duration. (b) The ln time versus $-n\ln(1-\xi)$ plot indicates the conformity of data points to the Avrami empirical law. The slope of the fitted line indicates n.

6. Discussion

6.1. Swelling behavior

Swelling structures have been reported in experiments on mafic compositions and attributed to metastable precursors of a chloritic phase, possibly smectite [20]. However, it should be noted that the expandable fraction found here grows with time at the expense of the non-expandable one: the longest run consists almost entirely of the expandable fraction. In our experiments then, the expandable fraction does not appear to be associated with metastability.

The swelling behavior observed in the 10Å phase upon acetone treatment is a peculiarity of this high-pressure phase since no expansion is known to occur in any clay mineral under acetone treatment. Furthermore the expansion observed in the 10Å phase (1.5 Å) is much smaller than that observed upon treatment of clays with other organic liquids. For example, kerolite, $R_3Si_4O_{10}(OH)_2{\cdot}n(H_2O)$, a hydrated species of talc [21] with R mainly Mg and $n \sim 0.8$–1.2, expands after several weeks of exposure to ethylene glycol by 7 Å to a basal spacing identical to that of stevensite-type smectites (17 Å).

Chemical reactions between water and acetone are unlikely to occur. On the contrary the high miscibility between the two compounds suggests that acetone may intercalate in pre-existing layers of water. This is known in layered metal oxides which intercalate water-miscible organics showing a slight expansion in basal plane spacing (A.H. Francis, personal communication). This process may involve a realignment of the hydrogen bonded network to accommodate the organic molecule.

As described above, we have found that the behavior of the 10Å phase upon acetone treatment is a function of the duration of the synthesis run. We interpret this behavior as a time-dependent transformation from a non-expandable fraction to an expandable fraction. Broad peaks are assigned to the expandable fraction while sharper reflections to the non-expandable fraction. With the assumption that structural modifications are reflected in the diffracted intensities, basal X-ray reflections were fit to a pseudo-Voight function. Quantitative determination of reaction progress was carried out starting from fitted integral areas of broad and sharp peaks (I_b and I_s, respectively). The fraction transformed from non-expandable to expandable fractions is given by the ratio $\xi = I_b/(I_b+I_s)$. The expandable phase fraction in very short duration syntheses is poorly constrained because of difficulties in deconvolving the two peaks uniquely.

The fraction transformed is plotted against time in Fig. 9a. The data show that the nucleation

period prior to the first appearance of expandable layers is short or absent and that the reaction is nearly complete for the longest duration syntheses. The apparent absence of a nucleation phase supports a continuous time-dependent structural rearrangement, a process that is appropriately described by the Avrami empirical law:

$$\xi = 1-\exp(-kt)^n \quad (1)$$

where ξ represents the fraction transformed, t is time, k is the rate constant (time^{-1}) and n is a constant. By linearizing Eq. 1 a plot of $\ln\ln(1-\xi)$ against $\ln t$ shows that the behavior of the 10Å phase conforms to the Avrami equation (Fig. 9b). The fit yields the parameters $k = 0.01$ h^{-1} and $n = 0.63$.

The slope (n) of the linear plot depends on the reaction mechanism [22]: a value of $n \sim 0.5$ is characteristic of diffusion-controlled kinetics (e.g. the dehydroxylation of kaolinite) while $n \sim 1$ indicates a phase boundary-controlled reaction (e.g. the dehydroxylation of brucite). Therefore the values of the Avrami equation parameters that we find suggest that the kinetics of the time-dependent transformation involving the 10Å phase are mainly controlled by diffusion rather than phase boundary reactions. We relate this process to a continuous time-dependent hydration mechanism involving the incorporation of water in the interlayer during synthesis. If this process is slow and not pervasive into the structure, hydration may be heterogeneous. Interaction with acetone, i.e. intercalation of acetone into the water layer, may only occur in that fraction that has incorporated sufficient interlayer water. There should be a critical amount of water beyond which acetone intercalation occurs and it must be greater than zero since the d-spacing of the non-expandable fraction (ranging from 9.64 to 10.07 Å) indicates that it too has some interlayer water. A continuous time-dependent hydration mechanism is further supported by optical and scanning electron microscopy (SEM) observations of the 10Å phase which show no evidence of two distinct phases.

This mechanism may also explain the wide variety of inconsistent claims for the water content of the 10Å phase. Even though the durations of previous successful 10Å phase synthesis do not exceed 11 h, the synthesis duration appears to be correlated with inferred water content of the 10Å phase. So for example, the smallest estimated water content, $0.65H_2O$ pfu, corresponds to a shorter synthesis time from 0.08 to 1 h performed by Wunder and Schreyer [11]. Run products of longer experiments, mostly from 1 to 2 h, carried out by Bauer and Sclar [10], result in higher water content, i.e. $1H_2O$ pfu. The highest water content proposed for the 10Å phase, i.e. $2H_2O$ pfu, is by Yamamoto and Akimoto [4] who ran experiments from 3 to 11 h. However, it should be noted that this issue is complicated by the possible unreliability of the water content determination, mainly concerning data not obtained by weight-loss experiments such as those of Yamamoto and Akimoto [4]. Furthermore, different pressure and temperature conditions together with different percentages of water added to the starting material (15 wt% in the present study; as high as 52 wt% in experiments performed by Wunder and Schreyer [11]) may influence synthesis results and further complicate any possible relation between water content incorporated into the structure of the 10Å phase and run duration.

6.2. *Raman active mode assignments (800–3800 cm^{-1})*

The Raman spectrum of the 10Å phase differs from that of talc in the Si–O stretching region (800–1100 cm^{-1}), in the OH stretching region (3200–3800 cm^{-1}), and in the appearance of a mode at 1593 cm^{-1}.

Raman frequencies related to the tetrahedral network support the interaction between tetrahedra and water molecules in the interlayer. The appearance of a third band in the Si–O stretching region indicates a lowering of the symmetry of the tetrahedral sheet or an interaction with interlayer water or both. Interaction with the interlayer is expected to be strongest for the bridging Si–O bonds, and weakest for the non-bridging Si–O bond. The silicon non-bridging stretching mode should then be recognized by comparison with the spectrum of talc and assigned to the frequency at 1058 cm^{-1}. The shift of this mode from 1055 in

talc to 1058 cm^{-1} in the 10Å phase may be related to a variation in the Si–O distance. A decrease of the Si–O distance may lead to a strengthening of the bond and therefore a shift towards higher frequencies. Symmetric stretching vibrations involving bridging oxygens are assigned for the 10Å phase to the modes at 909 and 992 cm^{-1}. Bridging Si–O frequencies are therefore split compared to talc and we interpret this as a result of interaction with interlayer water molecules. The lower frequencies with respect to talc (1018 cm^{-1}) may reflect a weakening of the bonds due to the interaction with interlayer water and a slight expansion of the six-fold tetrahedral ring in order to accommodate the molecule.

High-frequency modes in the 10Å phase may be assigned by comparison with spectra of hydrogen-bearing compounds. Bending modes and stretching modes of water molecules, hydronium ions and hydroxyl groups are Raman and IR active. The hydronium ion has two bending modes (ν_2 and ν_4) and two stretching modes (ν_1 and ν_3). IR spectra of the H_3O^+ ion in acid hydrates and aqueous mineral acids show a wide range of frequencies ([23] and references therein): ν_2 ranges from 1020 to 1205 cm^{-1}, ν_4 from 1620 to 1750 cm^{-1}, ν_1 from 2720 to 2900 cm^{-1} and ν_3 from 2780 to 3220 cm^{-1}. White and Burns [24] recognized hydronium in micaceous minerals uniquely on the basis of the stretching mode frequency at 3470 cm^{-1}. In crystal hydrates, water molecules have a bending mode (ν_2) that ranges from 1590 to 1670 cm^{-1} [25]. In minerals such as beryl and cordierite where the water molecule interacts weakly with the lattice, the symmetric and asymmetric stretching modes (ν_1 and ν_3) are found at 3555–3592 and 3632–3694 cm^{-1}, respectively [26]. In lawsonite, a strong interaction with the lattice lowers the symmetry of the water molecule and its vibrational eigenvectors and modifies the frequencies of O–H stretching considerably; observed frequencies are 2838 and 3612 cm^{-1} [27]. Vibrational frequencies of hydrogen bonds (O–H···O) depend on the bond length, with the highest frequencies ($\sim$3700 cm^{-1}) corresponding to the longest bonds (isolated hydroxyl) [28].

The Raman spectrum of the 10Å phase shows a weak peak at 1593 cm^{-1}. We assigned this peak to the bending mode (ν_2) of molecular water. This mode is absent in talc. The broad band at 3267 cm^{-1} is assigned to the first overtone ($2\nu_2$) of the fundamental bending mode of H_2O. In the OH stretching region only three peaks have been observed supporting a model structure with interlayer water. In fact the interaction between water molecules and basal tetrahedral oxygens suggest that water maintains its identity and forms three OH bonds: (1) the oxygen of the water molecule is hydrogen bonded to the hydroxyl; (2) and (3) each hydrogen of the water molecule is hydrogen bonded to one of the basal oxygens. Therefore, every OH bond we know must exist in the structure occupies a single structural site. This means that all hydroxyls must occupy symmetrically equivalent sites as must water molecules. The assignment of the three OH stretching modes is, however non-unique depending on the details of how the water molecules are accommodated into the structure. Their frequency will likely depend on the length of the O–H···O bond, with the highest frequency corresponding to the longest bond. The intense and sharp band at 3622 cm^{-1} is consistent with the hydroxyl stretching mode: the frequency is lowered compared to the hydroxyl stretch in talc by the formation of a hydrogen bond with interlayer water. The two lower intensity peaks at 3593 and 3668 cm^{-1} may be due to the stretching of O–H bonds of water molecules. The breadth of these signals may be associated with partial static disorder in the orientation of the water molecules.

It is worth noting that within or near the frequency ranges assigned in the literature to hydronium, we observed modes at 1055, 1593 and 3267 cm^{-1}. The first is attributed to non-bridging Si–O stretching, the second and the third to the bending mode of molecular water and its first overtone, respectively. Furthermore, among the three peaks in the OH stretching region, none agree with the stretching mode frequency of hydronium in micaceous minerals as reported by White and Burns [24] at 3470 cm^{-1}. Therefore, the presence of hydronium is not required from our observations.

Treatment with acetone produces a new peak in the Raman spectrum of the 10Å phase at 2923

cm^{-1}. The acetone molecule (CH_3COCH_3) has Raman active vibrations involving C–H bonds near 2900 cm^{-1} and a strong signal due to the double bond C=O at 1708 cm^{-1}. The signal observed in the Raman spectrum of treated 10Å phase at 2923 cm^{-1} may be assigned to C–H bonding. However, the absence of the intense C=O stretching mode may indicate an unfavorable orientation of the acetone molecule for Raman observation. Bauer and Sclar [10] observed by IR spectroscopy a mode at 1700 cm^{-1} that is absent in our spectra. The reason for this discrepancy is unclear. Although this mode was attributed by Bauer and Sclar [10] to hydronium bending, it is better explained by the double bond C=O, as discussed above, since contamination by acetone is indicated in Table 3 in Bauer and Sclar [10]. It is likely that the grain size of the sample may influence the observations: Bauer and Sclar [10] used a fine-grain sample (<5 μm) which may be randomly oriented with respect to the incident beam.

6.3. Unravelling the structure of 10Å phase

Powder X-ray diffractometry together with the Raman data suggests a model structure of the 10Å phase; the (100) projection is shown in Fig. 10. The model combines the mica-like stacking indicated by the X-ray data, with talc-like T–O–T sheets, and interlayer water molecules, as indicated by the Raman data. The model structure contains two water molecules pfu and satisfies the requirement of the Raman data that there be no more than three symmetrically distinct hydrogen bonds in the structure by relating the two water molecules with an inversion center. The water molecules are positioned so that they form three hydrogen bonds with the tetrahedral sheet as discussed above. Uncertainties in the model structure include the amount and detailed atomic positions of the water molecules. For example, it is possible that there be fewer than two water molecules pfu. The geometry of the model structure is such that the O–O distances between the water molecules are not large ($\sim$2.69 Å). Significant O–O repulsion would be expected at this distance, suggesting that a staggered arrangement of fewer water molecules may be energetically more favorable. We note that clay-like stacking of the T–O–T sheets would also reduce repulsion between the water molecules; however, the X-ray diffraction data appears to rule out this possibility.

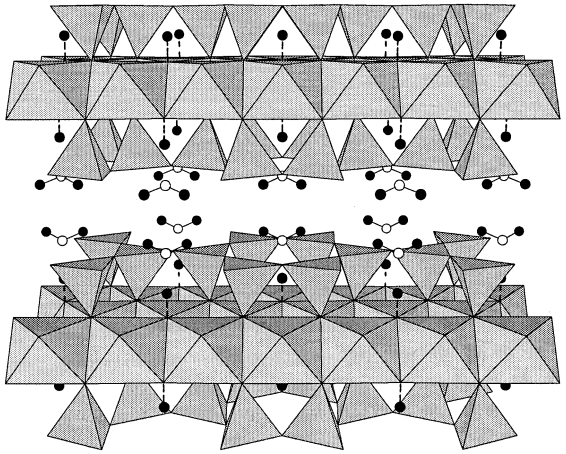

Fig. 10. (100) projection of the proposed model structure for the 10Å phase based on a phlogopite-type stacking with two water molecules in the interlayer. Open circles represent oxygens, filled circles represent hydrogens; dashed lines represent the hydrogen bonds relative to OH groups coordinated by magnesium.

X-ray powder diffractometry and Raman spectroscopy on treated samples demonstrate that the peculiar interaction with acetone is related to interlayer water further supporting the proposed model structure. The pre-existing water layer allows acetone to enter the structure and, due to its high miscibility in water, to intercalate within the interlayer. However, hydration of the 10Å phase is a time-dependent and not pervasive process. Incomplete hydration produces fractions within the structure which are more hydrated than others causing a differential behavior upon acetone treatment, making only the more hydrated fractions expandable. For our longest synthesis run, the hydration process appears to have been nearly completed as evidenced by the near absence of the, apparently metastable, non-expandable fraction.

Although we rule out the presence of hydronium by Raman observations, the interaction be-

tween interlayer water and OH groups, which are pointing towards the six-fold cavity of the tetrahedral sheets, may suggest a possible simultaneous occurrence of hydronium, water and hydroxyls as predicted by the resonating proton model [14]. However, the Raman spectrum would require the lifetime of hydronium to be short compared to the vibrational period. Invoking the presence of a resonating proton would add cohesive force to the structure but whether this additional force would be present in the case of short-lived hydronium is not predictable on the basis of present data.

Following on the idea of mica-like cohesive forces produced by complementary interlayer charge and charge-deficient layer, we have considered alternative structures for the 10Å phase that involve vacancies in the octahedral site. In such a case the stoichiometry would require Mg ions in the interlayer which would be hydrated and form more or less a continuous water shell. This model structure is similar to stevensites, which have been described as defective smectite structures caused by randomly distributed octahedral vacancies but no tetrahedral substitutions [29]. Random distribution of vacancies would explain the differential behavior of the 10Å phase upon acetone treatment. However, this alternative structure implies disorder in the octahedral site not recognized by Raman spectroscopy. The OH stretching frequency is very sensitive to the occupants of the octahedra, so that if vacancies were present, we would expect additional peaks compared to what is observed.

7. Implication for water transport along subduction zones

The ability of the 10Å phase to incorporate variable amounts of H_2O and the peculiar exchange ability of interlayer molecules open a number of possible scenarios on the role of the 10Å phase in subduction zone environments. Even though a maximum and unique H_2O content is expected in equilibrium at H_2O saturation (aqueous fluid present), our results suggest that H_2O-undersaturated conditions lead to a H_2O-deficient 10Å phase similar to some low-pressure minerals, e.g. cordierite.

It should be noted that the stability of such structures typical of 'low-temperature' environments to much higher temperature at high pressure is not uncommon and unpredictable. As an example lawsonite or pumpellyite structures, commonly observed at maximum temperatures of ca. 300°C in low-pressure metamorphism (see [30] for a review), were demonstrated to be stable to more than 800°C at pressures up to 10 GPa [31–33]. Even more relevant is the demonstration that fully hydrated montmorillonite is stable to 600°C under pressure conditions above the H_2O critical point [34].

The 10Å phase is not restricted to model compositions in the chemical system $MgO–SiO_2–H_2O$, but it occurs also in more complex systems approaching natural peridotites at least to pressures of 5.2 GPa and temperatures of 650°C [7,8]. In such Al-bearing systems, the 10Å phase appears to nucleate on chlorite and forms homogeneous

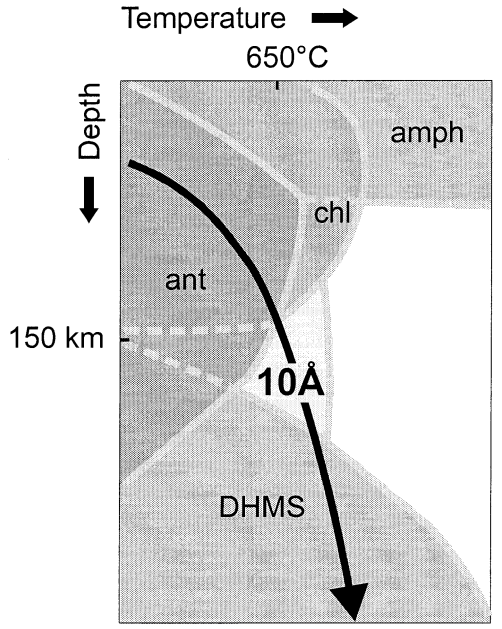

Fig. 11. Schematic phase diagram for a hydrous peridotite (after [7,8,32]) compared to a representative *P–T* path for subducted oceanic lithosphere. White field represents anhydrous peridotite assemblages.

macroscopic domains of chemical composition intermediate between clinochlore and talc. Notably, such composition corresponds to an unusual low-pressure, low-temperature phyllosilicate called kulkeite [35] composed of an ordered 1:1 sequence of chlorite/talc mixed-layers, which contains more than 12 wt% H_2O.

Even though it is well-established that the 10Å phase has an H_2O content significantly higher than talc, assuming $Mg_3Si_4O_{10}(OH)_2{\cdot}nH_2O$, where $0.65 < n < 2$, and $m = n+1$, fluid-absent reactions:

$$m\text{talc} = 10\text{Å } \textit{phase} + (1.5m-1.5)\text{enstatite} + (m-1)\text{coesite} \quad (2)$$

$$(0.25m + 2.5)\text{enstatite} + 0.125m\text{chlorite} = (0.5m + 1)\text{forsterite} + 0.25m\text{pyrope} + 10\text{Å } \textit{phase} \quad (3)$$

$$(1.5-0.25m)\text{enstatite} + 0.125m\text{chlorite} + (1 + 0.5m)\text{quartz} = 0.25m\text{pyrope} + 10\text{Å } \textit{phase} \quad (4)$$

easily explain the formation of the 10Å phase without addition of H_2O to the system, both in silica-undersaturated and silica-saturated systems. Such discontinuous reactions modeled in the system $MgO–Al_2O_3–SiO_2–H_2O$ actually correspond to complex continuous reactions in real systems which not only contain Fe but, above all, may display the complex behavior of the 10Å phase encountered in this study. Possible development of 10Å phase mixed-layer structures on talc and/or chlorite are responsible for complex $P–T–X^{X}_{Al}–X_{H_2O}$ loops governing a progressive breakdown of chlorite and/or talc with pressure and/or temperature increase. As a consequence, the dehydration process, if any (see Eqs. 2–4), related to the decomposition of chlorite (and/or talc) in subducted altered oceanic lithosphere does not result in a discrete fluid pulse from the slab to the mantle wedge but it corresponds to a continuous volatile release, smeared over a depth interval possibly 100 km large (Fig. 11). The stability of the 10Å phase mixed-layer structures may also promote H_2O transfer from the relatively low-pressure hydrous phases such as talc and chlorite to typical dense hydrous magnesian silicates, notably phase A via reactions of the form forsterite+10Å phase = phase A+enstatite [1]. Furthermore, as aqueous fluids released at eclogite facies conditions are expected to dissolve large amounts of Si and Al [36], but also Mg [37] as well as trace elements [38] the exchange properties of 10Å phase may drive element fractionation in a sort of chromatographic process. The ability of 10Å phase expandable structures to act as a sort of 'high-pressure molecular sieve' in subduction zone environments has still to be entirely explored and constitutes a stimulating perspective for future research.

Acknowledgements

Numerous discussions with Paola Comodi, Marcello Mellini, Gilberto Artioli and Don Peacor allowed us to improve earlier versions of the manuscript. We are indebted to P. Ulmer and to an anonymous referee for thoughtful and constructive reviews. We wish to thank Valeria Diella for assistance at the microprobe. Experimental and analytical work in Milan was funded by CNR (CSGAQ)-MURST (COFIN98). Experiments at the University of Michigan are supported by the US National Science Foundation under Grant EAR-9973050.*[AH]*

References

[1] P. Ulmer, V. Trommsdorf, Phase relations of hydrous mantle subducting to 300 km, in: Y.-W. Fei, C. Bertka, B.O. Mysen (Eds.), Mantle Petrology: Field Observations and High-Pressure Experimentation, The Geochemical Society, Special publication No. 6, 1999, pp. 259–281.

[2] J.G. Liou, R.Y. Zhang, Significance of ultrahigh-P talc-bearing eclogitic assemblages, Miner. Mag. 59 (1995) 93–102.

[3] C. Chopin, Talc-phengite: a widespread assemblage in high-grade pelitic blueschists of the Western Alps, J. Petrol. 22 (1981) 628–650.

[4] K. Yamamoto, S.I. Akimoto, The system MgO–SiO_2–H_2O at high pressures and temperatures-stability field for hydroxyl-chondrodite, hydroxyl-clinohumite and 10Å phase, Am. J. Sci. 277 (1977) 288–312.
[5] A.R. Pawley, B.J. Wood, The high-pressure stability of talc and 10Å phase: potential storage sites for H_2O in subduction zones, Am. Miner. 89 (1995) 998–1003.
[6] N.J. Chinnery, A.R. Pawley, S.M. Clark, In situ observation of the formation of 10Å phase from talc+H_2O at mantle pressures and temperatures, Science 286 (1999) 940–942.
[7] P. Fumagalli, S. Poli, Phase relationships in hydrous peridotites at high pressure: preliminary results of multianvil experiments, Period. Miner. 68 (1999) 275–286.
[8] P. Fumagalli, Processi di trasporto e rilascio di H_2O nelle zone di subduzione: uno studio sperimentale su sistemi ultrafemici ad alta pressione, Ph.D. Thesis, University of Milan, 2000.
[9] C.B. Sclar, L.C. Carrison, C.M. Schwartz, High-pressure synthesis and stability of a new hydronium-bearing layer silicate in the system MgO–SiO_2–H_2O, Trans. Am. Geophys. Union 46 (1965) 184.
[10] J.F. Bauer, C.B. Sclar, The '10Å phase' in the system MgO–SiO_2–H_2O, Am. Miner. 66 (1981) 576–585.
[11] B. Wunder, W. Schreyer, Metastability of the 10Å phase in the system MgO–SiO_2–H_2O (MSH). What about hydrous MSH phases in subduction zones?, J. Petrol. 33 (1992) 877–889.
[12] B. Wunder, W. Schreyer, Antigorite: high pressure stability in the system MgO–SiO_2–H_2O (MSH), Lithos 41 (1997) 213–227.
[13] O.Yu. Khodyrev, V.M. Agoshkov, Phase transitions in serpentine in the MgO–SiO_2–H_2O system at 40–80 kbar, Geochem. Int. 23 (1986) 47–52.
[14] A.K. Miller, S. Guggenheim, A.F. Koster Van Gross, The incorporation of 'water' in a high-pressure 2 layer silicate: a high pressure differential thermal analysis of the 10Å phase, Am. Miner. 76 (1) (1991) 106–112.
[15] D.L. Hamilton, C.M.B. Henderson, The preparation of silicate composition by gelling method, Miner. Mag. 36 (1968) 832–838.
[16] J. Zhang, B. Li, W. Utsumi, R.C. Liebermann, In situ X-ray observations on the coesite–stishovite transition: reversed phase boundary and kinetics, Phys. Chem. Miner. 23 (1996) 1–10.
[17] J. Susaki, S. Akaogi, O. Shimura, Garnet–perovskite transformation in $CaGeO_3$: in-situ X-ray measurements using synchrotron radiation, Geophys. Res. Lett. 12 (1985) 729–732.
[18] D.A. McKeown, M.I. Bell, E.S. Etz, Raman spectra and vibrational analysis of the trioctahedral mica phlogopite, Am. Miner. 84 (1999) 970–976.
[19] G.J. Rosasco, J.J. Blaha, Raman microprobe spectra and vibrational mode assignments of talc, Appl. Spectrosc. 34 (1980) 140–144.
[20] M.J. Apted, J.G. Liou, Phase relations among greenschist, epidote–amphibolite, and amphibolite in a basaltic system, Am. J. Sci. 283 (1983) 328–354.
[21] G.W. Brindley, D.L. Bish, H.M. Wan, The nature of kerolite, its relation to talc and stevensite, Miner. Mag. 41 (1977) 443–452.
[22] J.D. Hanckock, J.H. Sharp, Method of comparing solid-state kinetic data and its application to the decomposition of kaolinite, brucite, and $BaCO_3$, J. Am. Ceram. Soc. 55 (1972) 74–77.
[23] R.W.T. Wilkins, A. Mateen, G.W. West, The spectroscopic study of oxonium ions in minerals, Am. Miner. 59 (1974) 811–819.
[24] J.L. White, A.F. Burns, Infrared spectra of hydronium ion in micaceous minerals, Science 141 (1963) 800–801.
[25] G.V. Yukhnevich, Advances in the use of infrared spectroscopy for the characterization of OH bonds, Russ. Chem. Rev. 32 (1963) 619–633.
[26] R.D. Aines, G.R. Rosman, The high temperature behavior of water and carbon dioxide in cordierite and beryl, Am. Miner. 69 (1984) 319–327.
[27] E. Libowitzky, G.R. Rossman, FTIR spectroscopy of lawsonite, Am. Miner. 81 (1986) 1080–1091.
[28] K. Nakamoto, M. Margoshes, R.E. Rundle, Stretching frequencies as a function of distances in hydrogen bonds, J. Am. Chem. Soc. 77 (1955) 6480–6486.
[29] S. Shimoda, Mineralogical studies of a species of stevensite from the Obori mine, Yamagata Prefecture, Japan, Clay Miner. 9 (1971) 185–192.
[30] M. Frey, C. De Capitani, J.G. Liou, A new petrogenetic grid for low-grade metabasites, J. Metamorph. Geol. 9 (1991) 497–509.
[31] T. Fockenberg, An experimental study of the pressure–temperature stability of MgMgAl–pumpellyite in the system MgO–Al_2O_3–SiO_2–H_2O, Am. Miner. 83 (1998) 220–227.
[32] M.W. Schmidt, S. Poli, Experimentally based water budgets for dehydrating slabs and consequences for arc magma generation, Earth Planet. Sci. Lett. 163 (1998) 361–379.
[33] K. Okamoto, S. Maruyama, The high-pressure synthesis of lawsonite in the MORB+H_2O system, Am. Miner. 84 (1999) 362–373.
[34] W.A. Basset, T.C. Wu, I.-M. Chou, H.T. Haselton, J. Frantz, Jr., B.O. Mysen, W.L. Huang, S.K. Sharma, D. Schiferl, The hydrothermal diamond anvil cell (HDAC) and its applications, in: M.D. Dyar, C. McCammon, M.W. Schaefer (Eds.), Mineral Spectroscopy: a Tribute to Roger G. Burns, The Geochemical Society, Special Pubblication No. 5, 1996, pp. 261–272.
[35] W. Schreyer, O. Medenbach, K. Abraham, W. Gebert, W.F. Müller, Kulkeite, a new metamorphic phyllosilicate mineral: ordered 1 chlorite/talc mixed-layer, Contrib. Miner. Petrol. 80 (1) (1982) 103–109.
[36] C.E. Manning, Fluid composition at the blueschist–eclogite transition in the model system Na_2O–MgO–Al_2O_3–

SiO_2–H_2O–HCl, Schweiz. Miner. Petrogr. Mitt. 78 (1998) 225–242.

[37] R. Stalder, P. Ulmer, A.B. Thompson, D. Günther, High pressure fluids in the system MgO–SiO_2–H_2O under upper mantle conditions, Contrib. Miner. Petrol. (2000), in press.

[38] H. Keppler, Constraints from partitioning experiments on the composition of subduction-zone fluids, Nature 380 (1996) 237–240.